



Title	Dimensional and hydrodynamic properties of cellulose tris(alkylcarbamate)s in solution: Side chain dependent conformation in tetrahydrofuran
Author(s)	Jiang, XinYue; Ryoki, Akiyuki; Terao, Ken
Citation	Polymer. 2017, 112, p. 152-158
Version Type	AM
URL	<a href="https://hdl.handle.net/11094/71324">https://hdl.handle.net/11094/71324</a>
rights	© 2017, Elsevier. Licensed under the Creative Commons Attribution-NonCommercial-NoDerivatives 4.0 International <a href="https://creativecommons.org/licenses/by-nc-nd/4.0/">https://creativecommons.org/licenses/by-nc-nd/4.0/</a>
Note	

*The University of Osaka Institutional Knowledge Archive : OUKA*

<https://ir.library.osaka-u.ac.jp/>

The University of Osaka

Dimensional and hydrodynamic properties of cellulose  
tris(alkylcarbamate)s in solution: Side chain dependent conformation  
in tetrahydrofuran

XinYue Jiang, Akiyuki Ryoki, and Ken Terao\*

Department of Macromolecular Science, Osaka University, Department of Macromolecular  
Science, Osaka University, 1-1, Machikaneyama-cho, Toyonaka, Osaka 560-0043, Japan.

\* Corresponding author. Tel.: +81 6 6850 5459; fax +81 6 6850 5461

E-mail address: [kterao@chem.sci.osaka-u.ac.jp](mailto:kterao@chem.sci.osaka-u.ac.jp)

## ABSTRACT

We prepared cellulose tris(ethylcarbamate) (CTEC), cellulose tris(*n*-butylcarbamate) (CTBC), and cellulose tris(*n*-octadecylcarbamate) (CTODC) samples with different molecular weight to determine their conformational properties in dilute solution. Weight average molar masses  $M_w$ ,  $z$ -average mean-square radii of gyration  $\langle S^2 \rangle_z$ , particle scattering functions  $P(q)$ , and intrinsic viscosities  $[\eta]$  of the CTEC, CTBC, and CTODC samples in tetrahydrofuran (THF) at 25 °C were determined by size exclusion chromatography equipped with multi-angle light scattering detectors (SEC-MALS), small angle X-ray scattering (SAXS), and viscometry. Infrared (IR) absorption measurements were also made to observe intramolecular hydrogen bonding between C=O and NH groups. The obtained  $\langle S^2 \rangle_z$ ,  $P(q)$ , and  $[\eta]$  data were analyzed in terms of the wormlike chain model to determine the Kuhn segment length (stiffness parameter, or twice of the persistence length)  $\lambda^{-1}$  and the helix pitch (rise) per residue  $h$ . While CTBC has the highest chain stiffness in the three cellulose derivatives as in the case of the corresponding amylose derivatives, the difference in the wormlike chain parameters is less significant for the cellulose alkylcarbamate derivatives. Indeed, intramolecular hydrogen bonding of CTEC, CTBC, and CTODC is weaker and fewer than that for the corresponding amylose derivatives owing to the main chain linkage,  $\alpha$  or  $\beta$ .

Key Words: polysaccharide derivatives, wormlike chain, hydrogen bond.

## 1. Introduction

Cellulose tris(phenylcarbamate) (CTPC) was originally utilized to elucidate the conformational properties of cellulose ( $\beta$ -1,4-glucan) because hydroxyl groups of cellulose tend to form intermolecular hydrogen bonds with other cellulose molecules [1]. Dimensional and hydrodynamic properties of CTPC [2-7] can be explained by the Kratky-Porod wormlike chain model [8]. Consequently, it behaves as a typical semiflexible polymer in solution. According to the latest investigation of CTPC, the chain stiffness parameter  $\lambda^{-1}$  of the model (the Kuhn segment length or twice of the persistence length) was determined as 21 nm in tetrahydrofuran (THF) [6] and 16 nm in 1-methyl-2-pyrrolidone (NMP) [9]. Similar chain stiffness was also reported to be 16 nm in NMP for cellulose tris(3,5-dimethylphenylcarbamate) [10, 11] which is widely used for chiral stationary phase for liquid chromatography [12, 13]. These values are rather similar to those for cellulose, that is,  $\lambda^{-1} = 10$ -50 nm depending on solvents [14-23], cellulose myristate ( $\lambda^{-1} = 23$  nm) [24], and (cyanoethyl)(hydroxypropyl)cellulose ( $\lambda^{-1} = 29$  nm) [25].

We recently found that some derivatives of amylose ( $\alpha$ -1,4-glucan) have significant side chain dependent chain conformation. For example, amylose tris(*n*-butylcarbamate) (ATBC) and amylose tris(*n*-hexylcarbamate) (ATHC) form tightly wounded helical structure in THF with very high chain stiffness ( $\lambda^{-1} = 75$  nm) stabilized by the intramolecular hydrogen bonding between NH and C=O groups of the neighboring repeat units [26, 27]. This value is indeed about 20 times larger than that for amylose in dimethyl sulfoxide ( $\lambda^{-1} = 4$  nm) [28] and 3.6 times larger than that for amylose tris(phenylcarbamate) in 1,4-dioxane ( $\lambda^{-1} = 21$  nm) [29]. On the contrary, amylose tris(ethylcarbamate) (ATEC) has appreciably smaller  $\lambda^{-1}$  (= 33 nm) in THF, suggesting that the intramolecular interactions between main chain and alkyl side groups play an important role for the main chain conformation of polysaccharide derivatives

[27]. These results imply us to investigate cellulose alkylcarbamates since no dimensional and hydrodynamic data are available in our knowledge.

We thus synthesized three cellulose alkylcarbamates, that is, cellulose tris(ethylcarbamate) (CTEC), cellulose tris(*n*-butylcarbamate) (CTBC), and cellulose tris(*n*-octadecylcarbamate) (CTODC) of which chemical structures are shown in Fig. 1; note that CTEC and CTBC were originally synthesized by MacCormick et al. [30] and Schurig et al. [31], respectively. Dimensional and hydrodynamic properties in THF were studied to determine the wormlike chain parameters and furthermore to elucidate how alkyl carbamate groups affect the conformational properties of cellulose derivatives.

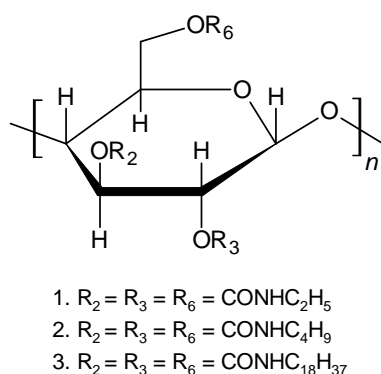


**Fig. 1.** Chemical structures of cellulose tris(ethylcarbamate) (1. CTEC), cellulose tris(*n*-butylcarbamate) (2. CTBC), and cellulose tris(*n*-octadecylcarbamate) (3. CTODC).

## 2. Experimental Procedures

### 2.1. Preparation of samples and their solutions

CTEC, CTBC, and CTODC samples were synthesized from commercially available cellulose powder (Wako, Japan) and micro crystalline cellulose (Sigma-Aldrich, USA) with an excess amount of corresponding isocyanate (ethylisocyanate, *n*-butylisocyanate, or *n*-

octadecylisocyanate) in a manner similar to that reported previously for cellulose [30] and amylose [26, 27, 32]. A typical procedure for a CTBC sample is as follows.

Cellulose (4 g, 0.025 mol) and LiCl (4 g) dried in vacuum at 80 °C for several hours were dissolved in *N,N*-dimethylacetamide (40 cm<sup>3</sup>) at 120 °C under argon atmosphere for 12 h. Distilled pyridine (100 cm<sup>3</sup>) and an excess amount of *n*-butylisocyanate (22 g, 0.22 mol) were added to the mixture and stirred by a magnetic bar to achieve complete reaction for 12 h at 120 °C under argon atmosphere. After the reaction, the mixture became a clear brown solution. The product was poured into a large amount of water to precipitate the crude CTBC sample. After drying in vacuum, a colorless fibrous sample was obtained. In the case of CTODC, twice amount of toluene was added to the reaction mixture to avoid gelation after adding the corresponding isocyanate. We have also attempted to prepare cellulose tris(*n*-hexylcarbamate) (CTHC) samples with *n*-hexylisocyanate because dilute solution properties of ATHC were reported [27]. We did not however use the CTHC samples in the following study because the crude product was not soluble in THF. *N,N*-dimethylacetamide (dehydrated grade, Wako), LiCl (Wako), ethylisocyanate (Wako), *n*-butylisocyanate (Wako), and *n*-octadecylisocyanate (Wako) were used without further purification while pyridine and toluene was purified by fractional distillation over CaH<sub>2</sub>.

The synthesized CTEC and CTBC samples were divided into several fractions by fractional precipitation with THF as solvent and water as precipitant. Similar procedure was also employed for CTODC with THF as solvent and methanol or acetone as precipitants. Appropriate middle fractions summarized in Table 2 as well as the unfractionated CTEC (CTEC-U) and CTBC (CTBC-U) samples were chosen for this study. Their chemical structures were confirmed by solution <sup>1</sup>H NMR spectra in CDCl<sub>3</sub>, IR absorption spectra, and elemental analysis. The weight ratio of nitrogen to carbon for each sample is consistent with

the theoretical value within 2%. The degree of substitution (DS) of CTEC and CTBC samples were estimated to be  $3.0 \pm 0.3$  from the ratio. The reprecipitated samples were dried in vacuum for more than 48 hours prior to preparation of THF solution. The solvent THF was distilled over CaH<sub>2</sub> except for the mobile phase of the size exclusion chromatography (SEC).

Solubility test of the CTEC, CTBC, and CTODC samples into various organic solvents was also performed to compare it with the corresponding amylose derivatives as summarized in Table 1. While CTBC, ATBC [26, 33], and ATEC [27] are soluble in various alcohols, CTEC has much less solubility in them other than methanol. This suggests that difference in the main chain linkage ( $\alpha$  or  $\beta$ ) significantly effects the solubility as is the case with the difference in cellulose and amylose. In the case of CTODC, the long side groups decrease the solubility into polar solvents while that in THF is good enough to determine dilute solution properties as discussed later.

**Table 1**

Solubility of cellulose and amylose alkylcarbamates in organic solvents at room temperature.

solvent	CTEC	ATEC <sup>a</sup>	CTBC	ATBC <sup>b</sup>	ATHC <sup>a</sup>	CTODC
chloroform	S	S	S	S	S	S
THF	S	S	S	S	S	S
methanol	S	S	S	S	I	I
2-propanol	I	S	S	S	I	I
1-propanol	I	S	S	S	S	I
2-butanol	I	S	S	S	S	I
1-butanol	I	S	S	S	S	I
2-ethoxyethanol	I	S	S	S	I	I

S: soluble. I: insoluble. ATEC: amylose tris(ethylcarbamate). ATBC: amylose tris(*n*-butylcarbamate). ATHC: amylose tris(*n*-hexylcarbamate). <sup>a</sup> Ref [27]. <sup>b</sup> Refs [26, 33].

## 2.2. Size exclusion chromatography with multi angle light scattering (SEC-MALS)

SEC-MALS measurements were made for the CTEC, CTBC, and CTODC samples to determine their weight-average molar mass  $M_w$  and the  $z$ -average mean-square radius of gyration  $\langle S^2 \rangle_z$  as a function of the elution volume  $V_e$  (Fig. 2). A TSKguardcolumn H<sub>XL</sub>-H column and a TSKgel H<sub>XL</sub> column are connected in series, and a sample loop with 100  $\mu$ L was used, and the flow rate was set to be 0.5 mL min<sup>-1</sup>. Mass concentration  $c$  of the injected solution were chosen to be  $2 \times 10^{-3} - 6 \times 10^{-3}$  g cm<sup>-3</sup>. A DAWN DSP multi-angle light scattering photometer and a refractive index detector were used to determine the Rayleigh ratio and  $c$  at each  $V_e$ , respectively. The refractive index increment  $\partial n/\partial c$  values at which the wavelength of the light scattering photometer ( $\lambda_0 = 633$  nm) in THF at 25 °C were determined to be 0.0841 cm<sup>3</sup> g<sup>-1</sup> for CTEC, 0.0872 cm<sup>3</sup> g<sup>-1</sup> for CTBC, and 0.0770 cm<sup>3</sup> g<sup>-1</sup> for CTODC. These values are substantially the same as those at the constant chemical potential for binary systems. The scattering data were extrapolated to infinite dilution and to zero angle with the aid of the Berry plot [34] because it shows good linearity both for flexible and rodlike chains at low  $q$  region [35]. It should be noted that the contribution from the second virial coefficient was negligibly small if we consider the value from SAXS measurements. The obtained  $M_w$  and the dispersity index  $D$  ( $\equiv M_w/M_n$  with  $M_n$  the number-average molar mass) for each sample except for the unfractionated samples (CTEC-U and CTBC-U) are shown in Table 2. These  $M_w$  values were at most 1 % larger than the uncorrected data at finite concentration. The second peak in Fig. 2 may show the scission of the main chain since the peak tends to become more appreciable with increasing side chain length.

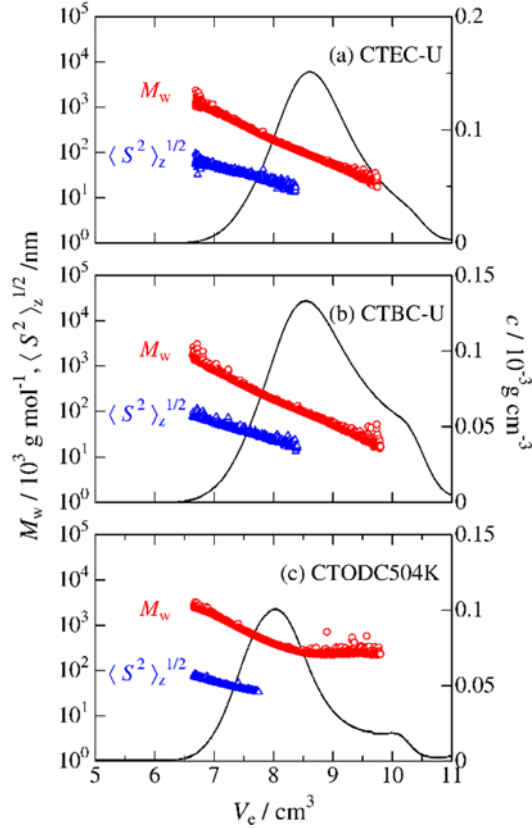


**Fig. 2.** Elution volume  $V_e$  dependence of the weight-average molar mass  $M_w$  (red circles), the  $z$ -average mean-square radius of gyration  $\langle S^2 \rangle_z^{1/2}$  (blue triangles), and the polymer mass concentration  $c$  (solid curves) for (a) CTEC-U and (b) CTBC-U, and (c) CTODC504K in THF.

### 2.3. Small-Angle X-ray Scattering (SAXS)

SAXS measurements were carried out for CTEC83K, CTEC68K, CTEC43K, CTBC64K, CTBC18K, CTODC89K, and CTODC35K in THF at 25 °C at the BL40B2 beamline in SPring-8 (Hyogo, Japan). Test solutions with four different concentrations ranging from  $4 \times 10^{-3}$  to  $2 \times 10^{-2} \text{ g cm}^{-3}$  were prepared for each sample. Solvent and solutions having different  $c$  were measured in a quartz glass capillary with a diameter of 2.0 mm. It should be noted that some preliminary measurements were also performed at the BL6A beamline in KEK-PF (Ibaraki, Japan) to estimate the measurement conditions (not shown in this paper). The wavelength,

camera length, and accumulation time were set to be 0.10 nm, 4000 mm, and 120-300 s, respectively. Two dimensional scattering intensity data were recorded by a RIGAKU R-AXIS VII imaging plate. The actual camera length was determined by means of the Bragg reflection of silver behenate. The circular average was utilized to obtain scattering intensity  $I(q)$  as a function of the magnitude of the scattering vector  $q$ . The background was measured from the scattering intensity of pure solvent in the exactly the same cell to determine the excess scattering intensity  $\Delta I(q)$ . The scattering intensities for each solution or solvent were corrected for the incident-beam intensity and the transmittance, both determined using the ionic chambers installed at the upper and lower ends of the capillary. The Berry square-root plots [34] were utilized to determine  $\langle S^2 \rangle_z$  and the particle scattering function  $P(q)$ . The second virial coefficients  $A_2$  were also estimated from the concentration dependence with the method as reported elsewhere [36].

#### 2.4. Viscometry

Solvent and solution viscosities for the CTEC43K, CTEC68K, CTEC83K, CTEC140K, CTBC64K, CTBC190K, CTBC254K, CTODC89K, CTODC346K, and CTODC504K in THF at 25 °C were measured using a Ubbelohde-type viscometer of which share rate is in the order of  $10^3 \text{ s}^{-1}$ . The intrinsic viscosity  $[\eta]$  and the Huggins constant  $k'$  were determined from the Huggins, Fuoss-Mead, and Billmeyer plots. The resultant  $k'$  values were between 0.43 and 0.50 for CTEC, between 0.41 and 0.53 for CTBC and, between 0.36 and 0.42 for CTODC, suggesting that THF is a good solvent for the three cellulose derivatives.

#### 2.5. Infrared (IR) absorption

IR absorption measurements were made for CTEC43K, CTBC190K and CTODC346K in THF at 25 °C on an FT/IR-4200 (JASCO) spectrometer with a solution cell made of  $\text{CaF}_2$  having 0.05 mm path length. Concentrations of the test solutions were set to be  $0.02 \text{ g cm}^{-3}$ .

### 3. Results

#### 3.1. Experimental results of the dimensional and hydrodynamic properties in THF

Fig. 3 illustrates  $q^2$  dependence of  $P(q)^{-1/2}$  for CTEC, CTBC, and CTODC samples in THF at 25 °C at low- $q$  range. The  $\langle S^2 \rangle_z^{1/2}$  values were determined from the initial slope and listed in Table 2, along with  $[\eta]$ . The average  $A_2$  values for relatively low molar mass CTEC, CTBC and CTODC were estimated from SAXS data to be  $1 \times 10^{-4}$ ,  $3 \times 10^{-4}$ , and  $2 \times 10^{-4} \text{ cm}^3 \text{ mol g}^{-2}$ , indicating that THF is a good solvent for the three cellulose carbamates as in the case of  $k'$ .

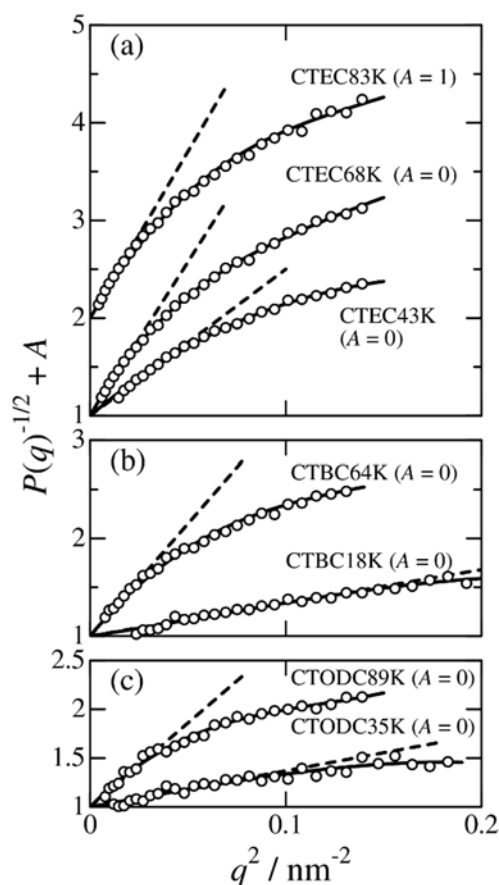


**Fig. 3.** Berry plots for indicated (a) CTEC, (b) CTBC, and (c) CTODC samples in THF at 25 °C. The ordinate values for CTEC83K are shifted by  $A$ . Dashed lines indicate the initial slopes to determine  $\langle S^2 \rangle_z$ .

**Table 2**

Molecular characteristics and physical properties of CTEC, CTBC, and CTODC samples in THF at 25 °C.

Sample	$M_w / 10^3 \text{ g mol}^{-1}$	$\bar{D}^a$	DS	$\langle S^2 \rangle_z^{1/2} / \text{nm}$	$[\eta] / \text{cm}^3 \text{g}^{-1}$
CTEC43K	43.3	1.5	3.0	9.49	46.0
CTEC68K	68.2	1.2	3.2	13.2	70.0
CTEC83K	82.5	1.6	3.3	14.3	75.0
CTEC140K	140	1.6	3.2	-	111
CTBC18K	17.8	1.3	3.2	4.52	
CTBC64K	64.4	2.1	3.3	11.7	59.0
CTBC190K	190	1.3	3.3	-	132
CTBC254K	254	1.3	3.2	-	197
CTODC35K	34.7	1.3	-	4.71	
CTODC89K	88.9	1.4	-	10.2	30.5
CTODC346K	346	1.3	-	-	99.0
CTODC504K	504	1.4	-	-	110

<sup>a</sup> Defined as  $M_w / M_n$

Molar mass dependence of  $\langle S^2 \rangle_z^{1/2}$  is displayed in Fig. 4 for CTEC, CTBC and CTODC in THF at 25 °C. The slope at lower  $M_w$  range for the three cellulose derivatives are 0.75, 0.78, and 0.82, and they decrease with increasing  $M_w$ . These are typical behavior for semirigid polymer chains in solution. Fig. 5 shows the experimental  $[\eta]$  data plotted against  $M_w$  for the three cellulose carbamates in THF. Their slopes are 0.81, 0.81, and 0.79 for CTEC, CTBC and CTODC, supporting the results from  $\langle S^2 \rangle_z^{1/2}$ .

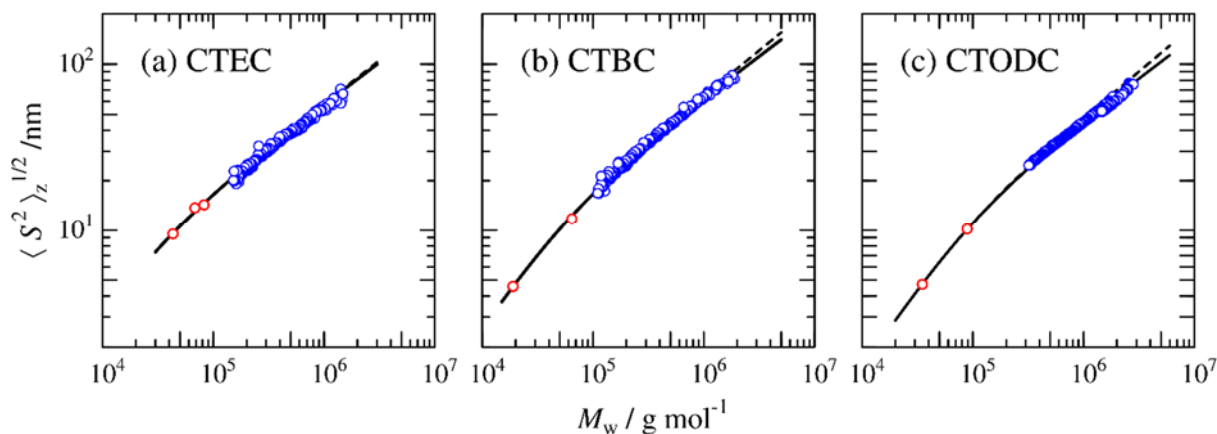


**Fig. 4.**  $M_w$  dependence of  $\langle S^2 \rangle_z^{1/2}$  for (a) CTEC, (b) CTBC, and (c) CTODC in THF at 25 °C. Blue and red circles are the experimental data determined from SEC-MALLS and SAXS measurements, respectively. Solid and dashed curves, theoretical values for the wormlike chains without and with excluded volume effects.

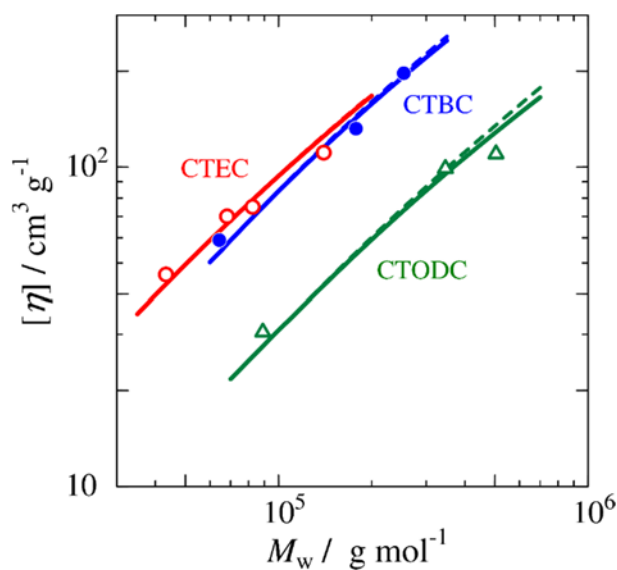


**Fig. 5.**  $M_w$  dependence of  $[\eta]$  for CTEC (unfilled circles), CTBC (filled circles), and CTODC (triangles) in THF at 25 °C. Solid and dashed curves, theoretical values for the wormlike chains without and with excluded volume effects.

The Holtzer plots [37] are suitable to analyze the particle scattering function of the semiflexible and rigid polymer chains in solution. The reduced Holtzer plots [ $M_w q P(q)$  vs  $q$ ]

for seven cellulose derivative samples in THF are illustrated in Fig. 6. For CTEC and CTBC samples, wide horizontal region so called ‘Holtzer plateau’ are found at high  $q$  range, indicating chain thickness is hardly effectible to the  $P(q)$  for the current system while a peak at lower  $q$  range reflects the finite chain stiffness. Monotonic increase behavior for CTODC at high  $q$  range is most likely due to the low electron density of the side alkyl groups comparing with the main chain and solvent. Similar behavior were also found for some other systems [38-40].

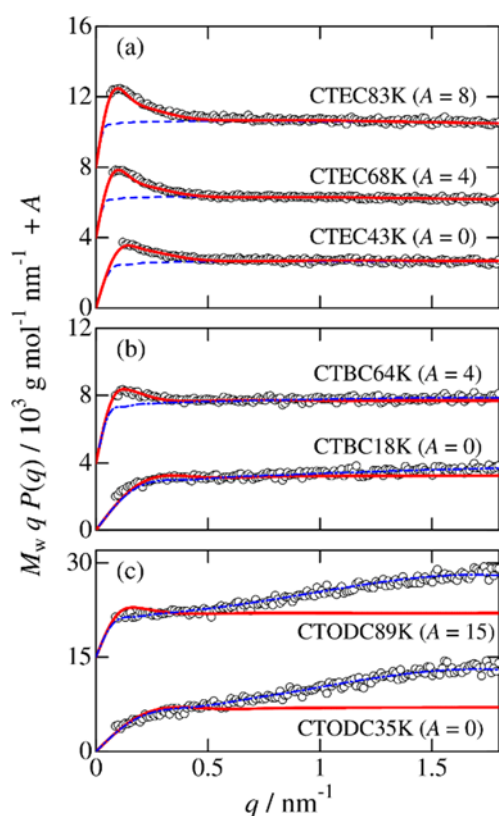


**Fig. 6.** Reduced Holtzer plots for the indicated CTEC, CTBC, and CTODC samples in THF at 25 °C. The ordinate values are shifted by  $A$ . Solid red curves, theoretical values for cylindrical wormlike chains with the parameters in Table 3. Dashed curves in panel (a), theoretical values for rigid cylinders. Dot-dashed curves in panels (b) and (c), theoretical values for core-shell cylinders. See text for the parameters.

### 3.2. Solution IR spectra

According to Kasat et al. [41, 42] intramolecular hydrogen bonds of C=O groups for 3,5-dimethylphenylcarbamate derivatives of cellulose and amylose are detectable from the amide I band in the IR spectra. We recently determined the number fraction  $f_{\text{hyd}}$  of hydrogen bonding C=O groups for amylose alkylcarbamates in solution [26, 27, 33]. Fig. 7 shows wavenumber dependence of the molar absorption coefficient  $\varepsilon$  for CTEC43K, CTBC190K, and CTODC346K in THF at 25 °C. Split amide I bands at 1742  $\text{cm}^{-1}$  and 1714  $\text{cm}^{-1}$  may be assigned as free and hydrogen bonding C=O groups. While the wavenumber of the former peak is almost equivalent to the corresponding amylose derivatives, the latter value is quite larger than those for ATEC (1700  $\text{cm}^{-1}$ ) and ATBC (1698  $\text{cm}^{-1}$ ), suggesting that the hydrogen bonds of CTEC and CTBC are somewhat weaker than those for the corresponding amylose derivatives. The observed double peaks are well fitted by the two Gaussian distributions as illustrated in the figure and therefore the values of  $f_{\text{hyd}}$  were estimated to be 0.42 (CTEC), 0.44 (CTBC), and 0.40 (CTODC).

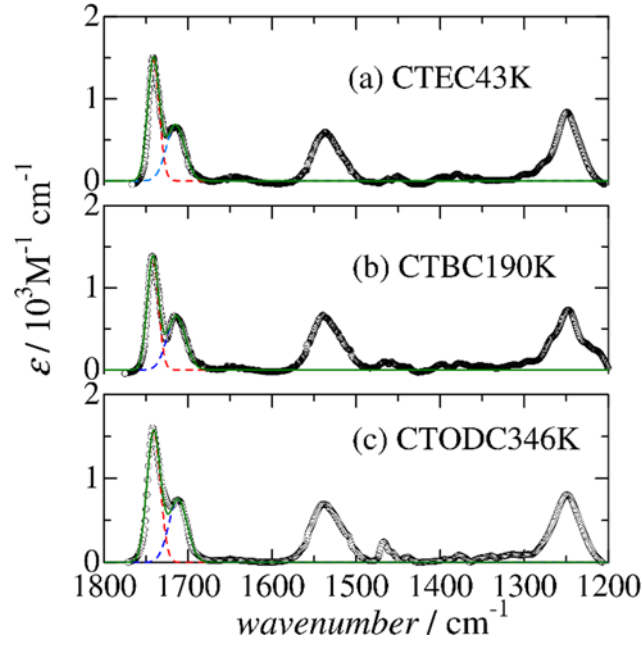


**Fig. 7.** Solution IR spectra for indicated cellulose carbamate derivative samples in THF at 25 °C.

## 4. Discussion

### 4.1. Analyses in terms of the wormlike chain model

All the dimensional and hydrodynamic properties summarized in the former section have a typical feature of rigid and/or semiflexible polymer chains. We thus analyzed the data in terms of the conventional Kratky-Porod wormlike chain model [8], which is a special case of the helical wormlike chain [43]. According to Benoit and Doty [43, 44], theoretical gyration radius  $\langle S^2 \rangle_0$  for the unperturbed wormlike chain is calculated by the following equation

$$\langle S^2 \rangle_0 = \frac{L}{6\lambda} - \frac{1}{4\lambda^2} + \frac{1}{4\lambda^3 L} - \frac{1}{8\lambda^4 L^2} [1 - \exp(-2\lambda L)] \quad (1)$$

where  $L$  is the contour length and  $\lambda^{-1}$  is the Kuhn segment length. The former parameter should be proportional to the molar mass  $M$  of the polymer and the relationship can be written as  $L = M / M_L$  with  $M_L$  being the molar mass per unit contour length. The two wormlike chain parameters,  $M_L$  and  $\lambda^{-1}$ , were unequivocally determined from the curve fitting procedure and summarized in Table 3. The resultant theoretical solid curves in Fig. 4 successfully reproduce the experimental data. The intramolecular excluded volume effects might not be negligible in the present case because the Kuhn segment number  $n_K (\equiv \lambda L)$  for the highest molar mass are 100, 60, and 60 for CTEC, CTBC, and CTODC. These values are slightly larger than that for the threshold value ( $n_K = 50$ ) at which the excluded volume effects become not negligible for neutral polymers (other than polyelectrolytes) in solution [45, 46]. This effect can be estimated by the Domb-Barrett equation [47] in the quasi-two-parameter (QTP) theory [43, 48, 49], which is established both for flexible and semiflexible polymer chains in solution [43, 45, 50]. The theoretical radius of gyration of the wormlike chains  $\langle S^2 \rangle$  in good solvent can be written as

$$\langle S^2 \rangle = \alpha_s^2 \langle S^2 \rangle_0 \quad (2)$$

The radius expansion factor  $\alpha_s$  can be calculated with the parameters of  $\lambda$ ,  $M_L$ , and the excluded volume strength  $B$  as a function of  $M$ . The last parameter  $B$  is roughly estimated in terms of the QTP scheme from the  $A_2$  data to be 0.2, 1.4, and 2.4 nm for CTEC, CTBC, and CTODC. The calculated  $\langle S^2 \rangle$  shown as the dashed curves in Fig. 4 are only slightly larger than those for the corresponding unperturbed values (solid curves) if we chose the  $B$  values from  $A_2$ . We thus conclude that the excluded volume effects are insignificant for the current  $\langle S^2 \rangle$  data.

The particle scattering function  $P(q)$  determined by SAXS for relatively low  $M_w$  samples were analyzed in terms of the Nakamura-Norisuye expression [51] for the cylindrical wormlike chains. Three parameters,  $L$ ,  $\lambda^{-1}$ , and the diameter of the cylinder  $d$ , were uniquely determined

by a curve fitting procedure for the three CTEC samples as shown in Fig. 6. The appreciable difference of the theoretical values between wormlike cylinder (solid curve) and the rigid cylinder (dashed curves) with the same  $L$  and  $d$  indicates the accuracy of  $\lambda^{-1}$ . Substantially the same theoretical values were obtained (not shown) if we calculate theoretical z-average particle scattering function with the  $\bar{D}$  value in Table 2 assuming log-normal distribution.

In the case of the  $P(q)$  data for CTBC and CTODC, peaks at low- $q$  range are less significant than those for CTEC samples. This is because the Kuhn segment number of these samples are estimated to be between 0.6 and 2.2 from the above-mentioned wormlike chain parameters while those for CTEC samples are higher (3.0 – 5.7), suggesting the finite flexibility are hardly effectible the  $P(q)$  data. Although monotonically increase behavior of  $qP(q)$  at higher  $q$  range cannot be explained by the cylindrical wormlike chains, it can be explained by the concentric double cylinder proposed by Livsey [52]. The particle scattering function of the model can be expressed as

$$P(q) = \int_0^{\pi/2} \left[ \frac{d_o^2 G(q, \theta, d_o) + f d_i^2 G(q, \theta, d_i)}{d_o^2 + f d_i^2} \right]^2 \sin \theta d\theta \quad (3)$$

with

$$G(q, \theta, d_x) = \frac{\sin \left[ \frac{qL}{2} \cos \theta \right] J_1 \left[ \frac{q d_x}{2} \sin \theta \right]}{\left[ \frac{qL}{2} \cos \theta \right] \left[ \frac{q d_x}{2} \sin \theta \right]} \quad (4)$$

and

$$f = \frac{\Delta\rho_i - \Delta\rho_o}{\Delta\rho_o} \quad (5)$$

where  $d_i$  and  $d_o$  are the diameter of the inner (or core) and outer (or shell) cylinders,  $\Delta\rho_i$  and  $\Delta\rho_o$  are the corresponding excess electron densities, and  $J_1$  is a first-order Bessel function of

the first kind. If we choose appropriate parameters, that is,  $L$ ,  $d_i$ ,  $d_o$ , and  $f$  (see Supporting information for the parameters), at least  $L$  may be unequivocally determined. The mean  $M_L$  value from the resultant  $L$  for different  $M_w$  samples are listed in Table 3. Somewhat smaller  $M_L$  values determined from  $\langle S^2 \rangle$  is likely due to the coarse-grained model or the molecular weight distribution. The theoretical dot-dashed curves in Fig. 6 successfully reproduce the experimental data other than the low  $q$  region of CTBC64K owing to the chain flexibility. Indeed, the theoretical values (solid curves) for a thin wormlike chain ( $d = 0$ ) with the same  $\lambda^{-1}$  from  $\langle S^2 \rangle$  fairly explain the experimental  $P(q)$  at  $q < 0.5 \text{ nm}^{-1}$ . It should be noted that the discrepancy in the range of  $q > 0.5 \text{ nm}^{-1}$  is likely due to the above-mentioned heterogeneous electron density profile in the thickness direction, thus reasonable.

**Table 3**

The molar mass per unit contour length  $M_L$ , the Kuhn segment length  $\lambda^{-1}$ , and the chain diameter  $d$  for CTEC, CTBC, and CTODC from the different methods.

Polymer	Method	$M_L / \text{nm}^{-1} \text{ g mol}^{-1}$	$\lambda^{-1} / \text{nm}$	$d / \text{nm}$
CTEC	$\langle S^2 \rangle_z$	$850 \pm 20$	$17 \pm 1$	
	$P(q)$	$830 \pm 70$	$16 \pm 1$	$0.6 \pm 0.2$
	$[\eta]$	$840^a$	$16.5^a$	1.3
CTBC	$\langle S^2 \rangle_z$	$1150 \pm 50$	$25 \pm 1$	
	$P(q)$	$1230 \pm 30$	$25^a$	
	$[\eta]$	$1150^a$	$25^a$	2.5
CTODC	$\langle S^2 \rangle_z$	$1850 \pm 170$	$24 \pm 3$	
	$P(q)$	$2230 \pm 150$	$24^a$	
	$[\eta]$	$2040^a$	$24^a$	3

<sup>a</sup> Assumed.

Intrinsic viscosity  $[\eta]$  data were analyzed in a similar way of  $\langle S^2 \rangle$ . Theoretical values of wormlike cylinders in the unperturbed state can be calculated in terms of the Yamakawa-Fujii-Yoshizaki theory [43, 53, 54] with the three parameters of  $M_L$ ,  $\lambda^{-1}$ , and  $d$  at fixed  $M$ . If we assume the mean  $M_L$  and  $\lambda^{-1}$  from  $\langle S^2 \rangle_z$  and  $P(q)$ , the last parameter  $d$  may be determined from the curve fitting procedure (solid curve in Fig. 5) and the resultant values are shown in Table 3. The excluded volume effects on  $[\eta]$  is insignificant if we estimate viscosity expansion factor  $\alpha_\eta^3$  by means of the QTP scheme [43, 48, 49] with the Barrett equation [55]; note that we utilized the excluded volume strength estimated from  $A_2$  as is the case with  $\langle S^2 \rangle_z$ . The resultant theoretical values plotted as dashed curves in Fig. 5 are mostly the same as those for the corresponding unperturbed values (solid curves). The obtained chain thickness is reasonable because they are fairly close to the corresponding amylose derivatives ( $d = 1.6 \text{ nm}$  for ATEC [27], and  $2.5 \text{ nm}$  for ATBC [26] determined by  $[\eta]$ ). We may therefore conclude that the three

physical properties, that is,  $\langle S^2 \rangle_z$ ,  $P(q)$ , and  $[\eta]$ , are consistently explained by the current theories for the wormlike chains. In other words, we successfully determined the wormlike chain parameters of the three cellulose alkylcarbamates with reasonable accuracy. The mean values of the wormlike chain parameters are summarized in Table 4 along with  $f_{\text{hyd}}$ . The helix pitch (or helix rise) per residue  $h$  was calculated from  $M_L$  with the relationship of  $h = M_0 / M_L$  with  $M_0$  being the molar mass of the repeat unit. This table includes literature values for cellulose tris(phenylcarbamate) (CTPC) [6], amylose carbamate derivatives [26, 27, 29, 56], and curdlan tris(phenylcarbamate) (CdTPC) [57].

**Table 4**

Comparison of  $\lambda^{-1}$ , helix pitch per residue  $h$ , and number fraction of intramolecular hydrogen bonding C=O groups  $f_{\text{hyd}}$  for polysaccharide carbamate derivatives in THF (or 1,4-dioxane) at 25 °C.

Main chain	Polymer	$\lambda^{-1}$ / nm	$h$ / nm	$f_{\text{hyd}}$	Ref.
$\beta$ -1,4-glucan	CTEC	$16.5 \pm 1$	$0.45 \pm 0.02$	0.42	This work
$\beta$ -1,4-glucan	CTBC	$25 \pm 1$	$0.40 \pm 0.02$	0.44	This work
$\beta$ -1,4-glucan	CTODC	$24 \pm 1$	$0.51 \pm 0.03$	0.40	This work
$\beta$ -1,4-glucan	CTPC <sup>a</sup>	$21 \pm 2$	$0.50 \pm 0.04$	–	[6]
$\alpha$ -1,4-glucan	A TEC	$33 \pm 3$	$0.36 \pm 0.02$	0.46	[27]
$\alpha$ -1,4-glucan	ATBC	$75 \pm 5$	$0.26 \pm 0.01$	0.52	[26]
$\alpha$ -1,4-glucan	ATHC	$75 \pm 2$	$0.29 \pm 0.02$	0.53	[27]
$\alpha$ -1,4-glucan	ATPC <sup>b</sup>	$22 \pm 2^e$	$0.34 \pm 0.02^e$	–	[29]
$\alpha$ -1,4-glucan	AAPC <sup>c</sup>	$21 \pm 2^e$	$0.34 \pm 0.02^e$	–	[56]
$\beta$ -1,3-glucan	CdTPC <sup>d</sup>	$57 \pm 5$	$0.39 \pm 0.02$	–	[57]

<sup>a</sup> Cellulose tris(phenylcarbamate). <sup>b</sup> Amylose tris(phenylcarbamate). <sup>c</sup> Amylose-2-acetyl-3,6-bis(phenylcarbamate). <sup>d</sup> Curdlan tris(phenylcarbamate). <sup>e</sup> In 1,4-dioxane.

#### 4.2. Main chain and side group dependent local helical structure and chain stiffness

The obtained chain stiffness of CTBC is 50% larger than that for CTEC and the  $h$  value is smaller than those for the other cellulose derivatives. This is similar behavior of the corresponding amylose derivatives. We may thus presume that the local helical structure of CTBC may be somewhat tighter than those for the other cellulose carbamate derivatives as in the case of ATBC. Slightly higher  $f_{\text{hyd}}$  of CTBC supports this suggestion. Another significant aspect is that CTODC has relatively large  $h$  and  $\lambda^{-1}$  values while  $f_{\text{hyd}}$  is somewhat smaller than those for CTEC and CTBC. This is most likely because bulkier side groups both extend and

stiffen the main chain of CTODC, considering that similar main chain stiffening were found for other polymers, such as polymethacrylates [58], polyolefins [59], and polysilanes [60, 61]. If we compare the main chain dependence of the chain stiffness, cellulose derivatives (CTEC, CTBC, and CTPC) have similar or smaller chain stiffness  $\lambda^{-1}$  and fewer intramolecular hydrogen bonds ( $f_{\text{hyd}}$ ) than those for the corresponding amylose (ATEC, ATBC, and ATPC) and curdlan derivatives (CdTPC) (see also [57]). This indicates that cellulose main chain ( $\beta$ -1,4-glucan) does not tend to form regular helical structure comparing with amylose ( $\alpha$ -1,4-glucan) and curdlan ( $\beta$ -1,3-glucan). The local helical structure of cellulose derivatives has indeed more extended ( $h = 0.40 - 0.51$  nm) than those for amylose (0.26 – 0.36 nm) and curdlan (0.39 nm). The lower solubility of cellulose alkylcarbamates, especially CTEC and cellulose tris(*n*-hexylcarbamate) (CTHC), is possibly due to the hydrogen bonding feature because the residual free polar groups of cellulose alkylcarbamates may tend to form intermolecular hydrogen bonds with other polymer chains.

## 5. Conclusion

The Kuhn segment length  $\lambda^{-1}$ , the helix pitch per residue  $h$ , and number fraction of intramolecular hydrogen bonds of C=O groups  $f_{\text{hyd}}$  in THF at 25 °C were determined for three cellulose alkylcarbamates (CTEC, CTBC, and CTODC) with different alkyl side chain length. The chain stiffness of CTBC has higher than that for CTEC as is the case with amylose derivatives, suggesting length of alkyl side chains plays an important role to form local helical structure. On the other hand, bulkier side groups of CTODC tend to stiffen and extend the main chain. The range of chain stiffness of investigated cellulose derivatives are in the range between 16 and 25 nm, which do not exceed the values known for cellulose and other cellulose derivatives as mentioned in Introduction. These results indicate that the intramolecular

hydrogen bonds between NH and C=O groups on the neighboring repeat units of cellulose alkylcarbamate derivatives somewhat stiffen the main chain but it is still insignificant comparing with other polysaccharide carbamate derivatives, that is, amylose and curdlan.

## Acknowledgment

We are grateful to Professor Takahiro Sato in Osaka University for fruitful discussion, to Dr. Noboru Ohta (SPring-8) and Dr. Noriyuki Igarashi (KEK) for SAXS measurements, and to Mr. Shota Arakawa and Mr. Fumihiro Maeda for providing solubility data for amylose derivatives in Table 1. The synchrotron radiation experiments were performed at the BL40B2 in SPring-8 with the approval of the Japan Synchrotron Radiation Research Institute (JASRI) (Proposal No. 2015B1100, 2016A1053, and 2016B1088) and at the BL-6A in KEK-PF under the approval of the Photon Factory Program Advisory Committee (No. 2015G543). This work was partially supported by JSPS KAKENHI Grant No. 25410130.

## References

1. Burchard W. Light Scattering from Polysaccharides as Soft Materials. In: Borsali R and Pecora R, editors. *Soft Matter Characterization*: Springer Netherlands, 2008. pp. 463-603.
2. Burchard W, Husemann E. *Makromol Chem* 1961;44:358-87.
3. Burchard W. *Makromol Chem* 1965;88:11-28.
4. Gupta AK, Marchal E, Burchard W, Benoit H. *Polymer* 1976;17:363-66.
5. Daňhelka J, Netopiliak M, Bohdanecký M. *J Polym Sci, Part B: Polym Phys* 1987;25:1801-15.
6. Kasabo F, Kanematsu T, Nakagawa T, Sato T, Teramoto A. *Macromolecules* 2000;33:2748-56.
7. Yanai H, Sato T. *Polym J* 2006;38:226-33.
8. Kratky O, Porod G. *Recl Trav Chim Pays-Bas* 1949;68:1106-22.
9. Norisuye T, Tsuboi A, Sato T, Teramoto A. *Macromol Symp* 1997;120:65-76.
10. Tsuboi A, Yamasaki M, Norisuye T, Teramoto A. *Polym J* 1995;27:1219-29.
11. Tsuboi A, Norisuye T, Teramoto A. *Macromolecules* 1996;29:3597-602.
12. Ikai T, Okamoto Y. *Chem Rev* 2009;109:6077-101.
13. Okamoto Y, Kawashima M, Hatada K. *J Chromatogr A* 1986;363:173-86.
14. Bianchi E, Ciferri A, Conio G, Cosani A, Terbojevich M. *Macromolecules* 1985;18:646-50.

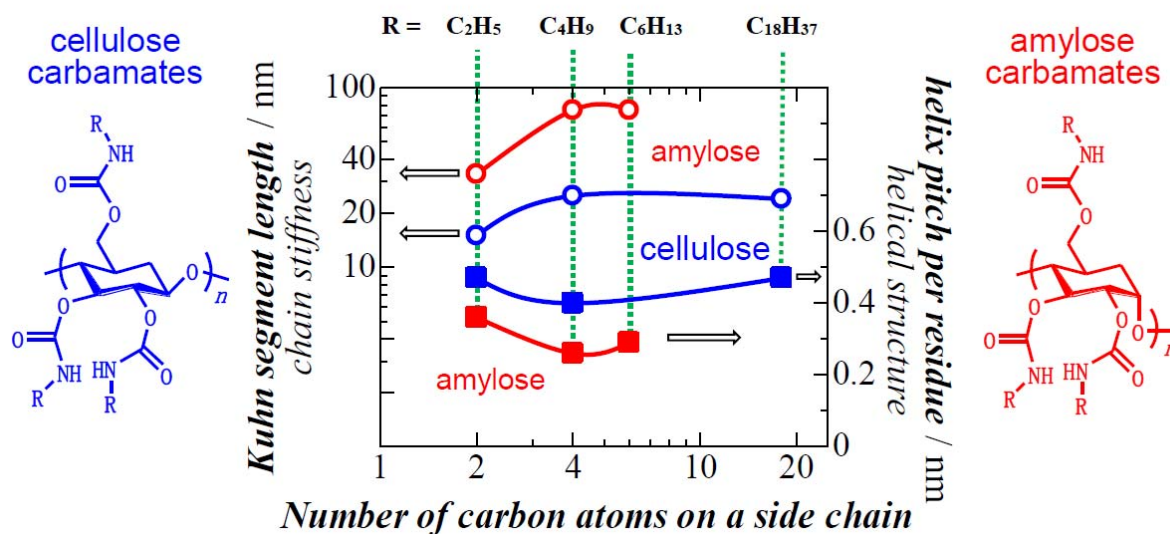
15. McCormick CL, Callais PA, Hutchinson BH. *Macromolecules* 1985;18:2394-401.
16. Kamide K, Saito M, Kowsaka K. *Polym J* 1987;19:1173-81.
17. Burchard W, Habermann N, Klüfers P, Seger B, Wilhelm U. *Angewandte Chemie International Edition in English* 1994;33:884-87.
18. Seger B, Aberle T, Burchard W. *Carbohydr Polym* 1996;31:105-12.
19. Saalwachter K, Burchard W, Klufers P, Kettenbach G, Mayer P, Klemm D, Dugarmaa S. *Macromolecules* 2000;33:4094-107.
20. Zhou JP, Zhang LN, Cai J. *J Polym Sci, Part B: Polym Phys* 2004;42:347-53.
21. Yanagisawa M, Isogai A. *Biomacromolecules* 2005;6:1258-65.
22. Cai J, Liu YT, Zhang LN. *J Polym Sci, Part B: Polym Phys* 2006;44:3093-101.
23. Kes M, Christensen BE. *J Chromatogr A* 2013;1281:32-7.
24. Bushin SV, Khripunov AK, Bezrukova MA, Astapenko EP. *Polymer Science Series A* 2007;49:71-76.
25. Mays JW. *Macromolecules* 1988;21:3179-83.
26. Terao K, Murashima M, Sano Y, Arakawa S, Kitamura S, Norisuye T. *Macromolecules* 2010;43:1061-68.
27. Terao K, Maeda F, Oyamada K, Ochiai T, Kitamura S, Sato T. *J Phys Chem B* 2012;116:12714-20.
28. Nakanishi Y, Norisuye T, Teramoto A, Kitamura S. *Macromolecules* 1993;26:4220-25.
29. Terao K, Fujii T, Tsuda M, Kitamura S, Norisuye T. *Polym J* 2009;41:201-07.
30. McCormick CL, Callais PA. *Polymer* 1987;28:2317-23.
31. Schurig V, Zhu J, Muschalek V. *Chromatographia* 1993;35:237-40.
32. Kubota T, Yamamoto C, Okamoto Y. *J Am Chem Soc* 2000;122:4056-59.
33. Sano Y, Terao K, Arakawa S, Ohtoh M, Kitamura S, Norisuye T. *Polymer* 2010;51:4243-48.
34. Berry GC. *J Chem Phys* 1966;44:4550-64.
35. Terao K, Mays JW. *Eur Polym J* 2004;40:1623-27.
36. Jiang XY, Terao K, Chung WJ, Naito M. *Polymer* 2015;68:221-26.
37. Holtzer A. *J Polym Sci* 1955;17:432-34.
38. Hickl P, Ballauff M, Scherf U, Mullen K, Linder P. *Macromolecules* 1997;30:273-79.
39. Terao K, Mizuno K, Murashima M, Kita Y, Hongo C, Okuyama K, Norisuye T, Bächinger HP. *Macromolecules* 2008;41:7203-10.
40. Arakawa S, Terao K, Kitamura S, Sato T. *Polym Chem* 2012;3:472-78.
41. Kasat RB, Zvinevich Y, Hillhouse HW, Thomson KT, Wang NHL, Franses EI. *J Phys Chem B* 2006;110:14114-22.
42. Kasat RB, Wee SY, Loh JX, Wang NH, Franses EI. *Journal of chromatography B, Analytical technologies in the biomedical and life sciences* 2008;875:81-92.
43. Yamakawa H, Yoshizaki T. *Helical Wormlike Chains in Polymer Solutions*, 2nd ed. Berlin, Germany: Springer, 2016.
44. Benoit H, Doty P. *J Phys Chem* 1953;57:958-63.
45. Norisuye T, Tsuboi A, Teramoto A. *Polym J* 1996;28:357-61.
46. Norisuye T, Fujita H. *Polym J* 1982;14:143-47.
47. Domb C, Barrett AJ. *Polymer* 1976;17:179-84.
48. Yamakawa H, Stockmayer WH. *J Chem Phys* 1972;57:2843-54.
49. Shimada J, Yamakawa H. *J Chem Phys* 1986;85:591-600.
50. Nakamura Y, Norisuye T. 2.02 - Polymer Properties in Solutions. In: Editors-in-Chief: Krzysztof M and Martin M, editors. *Polymer Science: A Comprehensive Reference*. Amsterdam: Elsevier, 2012. pp. 5-32.
51. Nakamura Y, Norisuye T. *J Polym Sci, Part B: Polym Phys* 2004;42:1398-407.
52. Livsey I. *Journal of the Chemical Society-Faraday Transactions Ii* 1987;83:1445-52.

53. Yamakawa H, Fujii M. *Macromolecules* 1974;7:128-35.
54. Yamakawa H, Yoshizaki T. *Macromolecules* 1980;13:633-43.
55. Barrett AJ. *Macromolecules* 1984;17:1566-72.
56. Tsuda M, Terao K, Kitamura S, Sato T. *Biopolymers* 2012;97:1010-17.
57. Ochiai T, Terao K, Nakamura Y, Yoshikawa C, Sato T. *Polymer* 2012;53:3946-50.
58. Xu Z, Hadjichristidis N, Fetters LJ. *Macromolecules* 1984;17:2303-06.
59. Fetters LJ, Lohse DJ, Garcia-Franco CA, Brant P, Richter D. *Macromolecules* 2002;35:10096-101.
60. Fujiki M, Koe JR, Terao K, Sato T, Teramoto A, Watanabe J. *Polym J* 2003;35:297-344.
61. Chung WJ, Shibaguchi H, Terao K, Fujiki M, Naito M. *Macromolecules* 2011;44:6568-73.

## Graphical Abstract

“Dimensional and hydrodynamic properties of cellulose tris(alkylcarbamate)s in solution:  
Side chain dependent chain conformation in tetrahydrofuran”

by XinYue Jiang, Akiyuki Ryoki, and Ken Terao\*



## Highlights

- Three cellulose alkylcarbamates (CTACs) with different side chain length behaves as semiflexible chains in solution.
- Solubility to common organic solvents is lower than those for amylose derivatives (ATACs) having the same side groups.
- Intramolecular hydrogen bonds is somewhat fewer than those for the corresponding ATACs in solution.
- Chain stiffness of the CTACs in solution is lower than that for the corresponding ATACs.
- More extended local helical structure was found comparing with ATACs.